Regular Article

ORGANIC CHEMISTRY RESEARCH
Published by the
Iranian Chemical Society
www.orgchemres.org

Org. Chem. Res., *Vol. 6, No. 1, 54-68, March 2020.*

$MnFe_2O_4$ MNPs Anchored Chitosan-Bu-SO_3H as a Recyclable Nanocatalyst for Sonochemical One Pot Heterocyclization of Indandione with Aniline and Acenaphthoquinone in Aqueous Media

H. Naeimi* and S. Lahouti

Department of Organic Chemistry, Faculty of Chemistry, University of Kashan, Kashan, 87317, I.R. Iran

(Received 24 November 2018, Accepted 8 April 2019)

In this research, the successful synthesis of spiro[acenaphthylene-1,9'-acridine] triones is described using 1,3-indandione, aniline and acenaphthoquinone in the presence of magnetic $MnFe_2O_4$@CS-Bu-SO_3H NPs catalyst under ultrasonic irradiation in water. The catalyst was fully characterized by scanning electronic microscopy (SEM), vibrating sample magnetometer (VSM), X-ray diffraction (XRD), thermal gravimetric analysis (TGA), energy dispersive X-ray (EDX), and Furrier transfer-infrared (FT-IR) spectroscopy. This method offers several advantages such as easy work-up, excellent yields, short reaction times, using of ultrasonic method, recoverability of the catalyst, and little catalyst loading.

Keywords: Ultrasound, Spiroheterocycles, Magnetic nanoparticles, $MnFe_2O_4$@CS-Bu-SO_3H, Chitosan, Five-component

INTRODUCTION

In the last few years, the application of ultrasound in synthetic organic chemistry has become more and more interesting because ultrasonic waves in liquids are known to cause chemical reactions either in homogeneous or in heterogeneous systems [1]. The chemical reactions are promoted by cavitation caused by ultrasonic waves traveling in the liquid. Here, cavitation implies the formation of micro-bubbles in a liquid subjected to sonication, which implode and generate high pressures and temperatures in their surrounding [2,3].

In general, sonication increases reaction rates and yields without using harsh conditions. Although there have been great deal of reports [4-6].

The presence of ultrasonic irradiation in a liquid-liquid system, cavitational falling near the liquid-liquid juncture interrupt the interface and induce of one liquid into the other forming emulsion, and leading to a dramatic increase in the interfacial contact area across which transfer of species can take place.

*Corresponding author. E-mail: naeimi@kashanu.ac.ir

Spiroheterocycles have remained relatively less investigated class of compounds until recent past.

The development of newer methods for their synthesis, however, has gained enormous attention especially in the area of organic as well as medicinal chemistry. Recently, being an important class of fused heterocycles and due to their wide range of pharmacological properties [7], spiroquinazolines have attracted a considerable interest in medicinal and pharmaceutical chemistry [8].

In recent years, applying heterogeneous catalysts in organic synthesis has become popular because they are removable from the reaction media by simple filtration and reusable [9].

In addition, to achieve high activity in heterogeneous catalysts, composite nanoparticles are the beneficial candidates because of their large surface to volume ratio, leading to an increase in catalytic activity. Furthermore, magnetic nanoparticles, especially supported magnetic nanocatalysts, have attracted a considerable interest in both academic and industrial research because they are viable alternatives to conventional materials, readily available, simple separation by an external magnet and high degree of chemical stability in various organic and inorganic solvents

[10-13] Chitosan is a very plentiful biopolymer achieved *via* the alkaline deacetylation of chitin [14].

It is applied widely in several industrial and manufacturing processes including wastewater treatment, pharmaceutical, medical, food processes, agriculture, and textile industries [15]. It has been used extensively not only as a catalyst for some reactions, but also as a support for the preparation of heterogeneous catalysts. The insertion of metals, into the chitosan polymer matrix may improve its capacity of interaction by complexation. Chitosan based composites are increasingly important as biochemical, antimicrobial, and catalytic reagents [16,17]. Compared with other ferrites, $MnFe_2O_4$ nanoparticles are relatively stable, and their high saturation magnetization will be favourable for sludge separation. In recent years, we have used ultrasound irradiation in organic synthesis [18-23]. Herein, we hope to report an efficient ultrasound-assisted eco-friendly protocol for the synthesis of spiro[acenaphthylene-1,9'-acridine] triones in the presence of magnetic $MnFe_2O_4$@CS-Bu-SO_3H NPs as a heterogeneous catalyst in aqueous media. The high yields, and the possibility of easy recovering of the catalyst are the most advantages of this method.

EXPERIMENTAL

Materials

The chemicals used in this work were obtained from Fluka and Merck Chemical Companies and were used without purification.

Apparatus

FT-IR spectra were obtained with potassium bromide pellets in the range of 400-4000 cm^{-1} with a Perkin-Elmer 550 spectrometer. ^1H NMR and ^{13}C NMR spectra were recorded with a Bruker DRX-400 spectrometer at 400 and 100 MHz, respectively. NMR spectra were reported as parts per million (ppm) downfield from tetramethylsilane as internal standard. The abbreviations used are: singlet (s), doublet (d), triplet (t) and multiplet (m). Nanostructures were characterized using a Holland Philips Xpert X-ray powder diffraction (XRD) diffractometer (CuK, radiation, k = 0.154056 nm), at a scanning speed of 2°/min from 10° to 100° (2ɵ). A BANDELIN ultrasonic HD 3200 with probe model KE 76, with the diameter of 6 mm, was used to produce ultrasonic irradiation and homogenizing the reaction mixture. Piezoelectric crystal of this kind of probe normally works in the range of 700 kHz; however, the output frequency of piezoelectric crystal is controlled and reduced to 20 kHz, using some proper clamps. Therefore, the induced frequency of probe to the reaction mixture is equal to 20 kHz. A thermal method was used for the calibration of ultrasonic power. Melting points were determined in open capillaries using an Electrothermal Mk3 apparatus and are uncorrected. The purity determination of the substrates and reaction monitoring were accomplished by TLC on silica-gel polygram SILG/UV 254 plates (from Merck Company). FE-SEM images of the products were visualized by a Sigma ZEISS, Oxford instruments field emission scanning electron microscope. The magnetic properties of nanoparticles were measured with a vibrating sample magnetometer (VSM, PPMS-9T) at 300 K in Iran (University of Kashan).

Typical Experimental Procedure for the Preparation of Chitosan-coated Magnetic Nanoparticles $MnFe_2O_4$@CS MNPs

$MnFe_2O_4$ MNPs were synthesized according to a previously reported procedure by chemical co-precipitation method [24] and subsequently were functionalized with chitosan [25]. In this research, the $MnFe_2O_4$ nanoparticles were prepared by following the reported standard protocol by co-precipitation of $MnCl_2$ and $FeCl_3$ in water in the presence of sodium hydroxide. Briefly, $MnCl_2.4H_2O$ and $FeCl_3.6H_2O$ were taken in molar ratio of Mn^{2+}: Fe^{3+} = 1:2 to prepare 0.4 M metal ion solution of 100 ml containing 0.2 M Mn^{2+} and 0.4 M Fe^{3+}, which was then dropped slowly into 100 ml NaOH solution of 5 M at the temperature of 97 °C. After aging for 2 h with continuous stirring, the mixture was filtered, washed and dried at 60 °C for 24 h. Next, the reaction mixture was cooled and the catalyst was isolated in the magnetic field and washed three times with distilled water. Subsequently, in order to prepare $MnFe_2O_4$-chitosan nanoparticles, 1 g of the $MnFe_2O_4$ nanoparticles was dispersed in 120 ml distilled water under ultrasound irradiation and 0.5 g of chitosan in 120 ml of 2.0 wt% acetic acid solution was slowly added under vigorous stirring at 50 °C for 1 h. The modified

$MnFe_2O_4$-chitosan nanoparticles were recovered by magnetic decantation and washed with CH_2Cl_2. Finally, $MnFe_2O_4$-chitosan nanoparticles were dried at 60 °C.

Preparation of 1,4-Butane Sultone Chitosan Encapsulated Manganese Ferrite Nanoparticles $MnFe_2O_4$@CS-Bu-SO_3H MNPs

The $MnFe_2O_4$-CS nanoparticles and 1,4-butane sultone (0.36 ml, 3 mmol) were mixed together without solvent and stirred 3 h at room temperature (25 °C) The concentrated H_2SO_4 (0.154 ml, 3 mmol) was added to the mixture of above catalyst and reflux for 2 h. The final catalyst was then washed repeatedly with ethanol and then dried (Scheme 3).

In order to determine the acid strength of catalyst, a 0.08 M solution of sodium hydroxide was used for measurement of total surface acidity for the $MnFe_2O_4$@CS-Bu-SO_3H MNPs. Then, 0.02 g of solid was suspended in this solution for 18 h, and the excess amount of base was titrated against the hydrochloric acid using phenolphthalein as an indicator. However, the number of H^+ sites for the catalyst structure was quantitatively determined about 0.36 mmol g^{-1}.

General Procedure for the Synthesis of Spiroacridines Catalyzed by $MnFe_2O_4$@CS-Bu-SO_3H MNPs under Ultrasound Irradiation

A mixture of dimedone (1) (2 mmol), aniline (2) (1 mmol), acenaphthoquinone (3) (1 mmol) and functionalized) $MnFe_2O_4$@CS-Bu-SO_3H MNPs (3 mol%) as a catalyst was added to a mixture of water and EtOH (5:1) (6 ml) as solvent and the reaction mixture was sonicated in ultrasonic apparatus with 40 Watt power. The progress of the reaction was monitored by TLC. The reaction mixture was filtered and the precipitate was washed with ethanol. The crude solid product was recrystallized from ethanol to give pure spiroacridine as a target product. Then, all of the products were identified by IR, ^{1}H NMR, ^{13}C NMR and C.H.N analyses.

Representative Spectral Data

(4-Nitrophenyl) spiro[acenaphthylene-1,9'-acridine] trione (4a). Orange solid, m. p. > 300 °C. IR (KBr) υ: 3610, 3475, 3358, 2961, 1717, 1612 cm^{-1}; ^{1}H NMR (400 MHz, DMSO-d_6) δ: 8.09 (d, 2H, ArH), 7.20-7.94 (m, 7H, ArH), 6.84 (s, 1H, ArH), 1.56-2.31 (m, 8H, $4CH_2$), 0.88-1.25 (m, 12H, $4CH_3$) ppm; ^{13}C NMR (100 MHz, DMSO-d_6) δ: 26.4, 30.5, 41.1, 46.2, 55.8, 106.9, 114.2, 116.7, 121.2, 123.6, 125.3, 126.5, 127.1, 130.6, 131.7, 132.6, 133.5, 135.2, 141.1, 152.5, 156.4, 159.6, 192.3, 202.5, 204.7 ppm. Anal. Calcd. for $C_{34}H_{30}N_2O_5$: C, 74.71; H, 5.53; N, 5.12. Found: C, 74.59; H, 5.61; N, 4.98.

(4-Hydroxyphenyl) spiro[acenaphthylene-1,9'-acridine] trione (4b). Orange solid, m. p. > 300 °C. IR (KBr) υ: 3613, 3460, 3347, 2932, 1710, 1617 cm^{-1}; ^{1}H NMR (400 MHz, DMSO-d_6) δ: 8.73 (d, 2H, ArH), 8.26 (t, 3H, ArH), 7.93 (d, 2H, ArH), 7.89 (s, 1H, OH), 7.12 (d, 2H, ArH), 6.82-7.33 (d, 2H, ArH), 1.75-2.32 (m, 8H, $4CH_2$), 0.95-1.14 (m, 12H, $4CH_3$) ppm; ^{13}C NMR (100 MHz, DMSO-d_6) δ: 27.8, 32.5, 41.1, 45.2, 54.8, 105.9, 112.2, 115.7, 120.2, 122.6, 124.3, 126.7, 127.2, 130.8, 131.5, 132.7, 134.5, 136.2, 142.1, 154.5, 158.4, 159.1, 193.3, 203.5, 204.4 ppm. Anal. Calcd. for $C_{34}H_{31}NO_4$: C, 78.89; H, 6.04; N, 2.71. Found: C, 78.81; H, 5.93; N, 2.59.

(4-Chlorophenyl) spiro[acenaphthylene-1,9'- acridine] trione (4c). Orange solid, m. p. > 300 °C. IR (KBr) υ: 3358, 2961, 2870, 1723, 1609 cm^{-1}; ^{1}H NMR (400 MHz, DMSO-d_6) δ: 6.95-8.86 (m, 10H, ArH), 1.60-2.22 (m, 8H, $4CH_2$), 0.75-1.14 (m, 12H, $4CH_3$) ppm; ^{13}C NMR (100 MHz, DMSO-d_6) δ: 27.9, 32.5, 42.1, 48.2, 57.8, 108.9, 112.2, 115.7, 121.2, 122.6, 124.3, 126.5, 129.1, 130.6, 131.8, 132.6, 134.5, 135.2, 140.1, 154.5, 158.4, 158.6, 189.3, 201.5, 203.7 ppm. Anal. Calcd. for $C_{34}H_{30}NO_3Cl$: C, 76.18; H, 5.64; N, 2.61. Found: C, 76.05; H, 5.72; N, 2.75.

(4-Bromophenyl) spiro[acenaphthylene-1,9'- acridine] trione(4d). Orange solid, m. p. > 300 °C. IR (KBr) υ: 3362, 2942, 2854, 1712, 1626 cm^{-1}; ^{1}H NMR (400 MHz, DMSO-d_6) δ: 8.26 (d, J = 7.2 2H, ArH), 7.81 (d, J = 7.2, 5H, ArH), 7.56 (d, J = 7.2, 2H, ArH), 7.21 (s, 1H, ArH), 1.70-2.36 (m, 8H, $4CH_2$), 0.96-1.10 (m, 12H, $4CH_3$) ppm; ^{13}C NMR (100 MHz, DMSO-d_6) δ: 27.1, 33.5, 40.1, 47.2, 55.8, 107.9, 111.2, 114.7, 120.2, 123.6, 125.3, 127.5, 128.1, 129.6, 132.8, 133.6, 134.7, 136.2, 140.7, 157.5, 158.4, 159.6, 190.3, 202.5, 205.7 ppm. Anal. Calcd. for $C_{34}H_{30}NO_3Br$: C, 70.35; H, 5.21; N, 2.41. Found: C, 70.22; H, 5.10; N, 2.30.

(p-Tolyl) spiro[acenaphthylene-1,9'-acridine] trione (4e). Orange solid, m. p. > 300 °C. IR (KBr) υ: 3451, 3143, 2940, 1662, 1606 cm^{-1}; ^{1}H NMR (400 MHz, DMSO-d_6) δ: 8.33 (s, 1H, ArH), 8.25 (d, J = 7.2 Hz, 2H, ArH), 7.92 (t, J = 7.2 Hz, 2H, ArH), 7.43-7.73 (m, J = 7.2 Hz, 3H, ArH), 7.28

(d, *J* = 7.8 Hz, 2H, ArH), 7.10 (d, *J* = 7.8 Hz, 1H, ArH), 2.51-2.84 (m, 8H, $4CH_2$), 2.43(s, 3H, CH_3), 0.85-1.12 (m, 12H, $4CH_3$) ppm; ^{13}C NMR (100 MHz, DMSO-d_6) δ: 28.2, 32.1, 47.1, 51.4, 54.8, 57.3, 108.7, 112.1, 119.3, 121.8, 124.0, 125.5, 127.9, 128.9, 130.6, 131.1, 133.6, 135.8, 138.7, 141.0, 157.6, 158.1, 165.6, 192.3, 205.5, 207.7 ppm. Anal. Calcd. for $C_{35}H_{33}NO_3$: C, 81.52; H, 6.45; N, 2.72. Found: C, 81.38; H, 6.34; N, 2.61.

(4-Methoxyphenyl) spiro[acenaphthylene-1,9'-acridine] trione (4f). Orange solid, m. p. > 300 °C. IR (KBr) υ: 3371, 3043, 2908, 1688, 1603 cm^{-1}; ^{1}H NMR (400 MHz, DMSO-d_6) δ: 8.55 (s, 1H, ArH), 8.15 (d, *J* = 7.2 Hz, 2H, ArH), 7.90 (t, *J* = 7.2 Hz, 2H, ArH), 7.52-7.79 (m, *J* = 7.2 Hz, 5H, ArH), 7.09 (d, *J* = 7.8 Hz, 2H, ArH), 6.93 (d, *J* = 7.8 Hz, 2H, ArH), 3.89 (s, 3H, OCH_3), 1.79-2.34 (m, 8H, $4CH_2$), 0.88-1.12 (m, 12H, $4CH_3$) ppm; ^{13}C NMR (100 MHz, DMSO-d_6) δ: 27.2, 33.1, 44.1, 51.2, 55.8, 56.3, 109.7, 113.1, 117.3, 121.1, 122.0, 125.2, 128.9, 129.9, 130.6, 131.8, 132.6, 135.7, 136.7, 142.0, 156.6, 158.6, 159.6, 190.3, 204.5, 206.7 ppm. Anal. Calcd. for $C_{35}H_{33}NO_4$: C, 79.07; H, 6.26; N, 2.63. Found: C, 78.94; H, 6.19; N, 2.69.

(2-Hydroxyphenyl) spiro[acenaphthylene-1,9'-acridine] trione (4g). Orange solid, m. p. > 300 °C. IR (KBr) υ: 3513, 3454, 3347, 2942, 1715, 1625 cm^{-1}; ^{1}H NMR (400 MHz, DMSO-d_6) δ: 7.76 (s, 1H, ArH), 7.73 (s, 1H, ArH), 7.65 (d, *J* = 7.2, 2H, ArH), 7.59 (d, *J* = 7.2, 2H, ArH), 7.44 (s, 1H, ArH), 7.42 (s, 1H, ArH), 7.41 (s, 1H, ArH), 7.39 (s, 1H, ArH), 7.37 (s, 1H, ArH), 2.45 (s, 2H, CH_2), 2.26 (s, 2H, CH_2), 2.15 (s, 2H, CH_2), 1.83 (s, 2H, CH_2), 0.98-1.10 (m, 12H, $4CH_3$) ppm; ^{13}C NMR (100 MHz, DMSO-d_6) δ: 28.8, 31.5, 40.1, 44.2, 52.8, 107.9, 113.2, 114.7, 119.2, 122.6, 125.3, 126.7, 128.2, 130.8, 132.5, 132.7, 135.5, 136.7, 144.1, 156.5, 158.1, 159.4, 192.3, 202.5, 205.4 ppm. Anal. Calcd. for $C_{34}H_{31}NO_4$: C, 78.89; H, 6.04; N, 2.71. Found: C, 78.81; H, 5.93; N, 2.59.

(2-Nitrophenyl) spiro[acenaphthylene-1,9'-acridine] trione (4h). Orange solid, m. p. > 300 °C. IR (KBr) υ: 3604, 3460, 3351, 2942, 1719, 1609 cm^{-1}; ^{1}H NMR (400 MHz, DMSO-d_6) δ: 7.26-8.09 (m, 10H, ArH), 2.01-2.15 (m, 8H, $4CH_2$), 0.90-1.20 (m, 12H, $4CH_3$) ppm; ^{13}C NMR (100 MHz, DMSO-d_6) δ: 27.1, 31.5, 44.1, 45.2, 52.8, 108.9, 113.2, 118.7, 120.2, 122.6, 125.4, 126.1, 128.1, 129.6, 131.7, 132.4, 134.5, 135.7, 142.1, 153.5, 155.4, 158.6, 193.3, 203.5, 205.7 ppm. Anal. Calcd. for $C_{34}H_{30}N_2O_5$: C, 74.71; H, 5.53; N, 5.12. Found: C, 74.59; H, 5.61; N, 4.98.

(2-Chlorophenyl) spiro[acenaphthylene-1,9'- acridine] trione (4i). Orange solid, m. p. > 300 °C. IR (KBr) υ: 3348, 2967, 2855, 1714, 1611 cm^{-1}; ^{1}H NMR (400 MHz, DMSO-d_6) δ: 8.42 (d, 2H, ArH), 8.09 (s, 1H, ArH), 7.95 (d, 3H, ArH), 7.90 (d, 2H, ArH), 7.83 (d, 2H, ArH), 2.25 (s, 8H, $4CH_2$), 0.75-1.10 (m, 12 H, $4CH_3$) ppm; ^{13}C NMR (100 MHz, DMSO-d_6) δ: 28.5, 31.5, 43.1, 46.2, 58.8, 110.9, 111.5, 114.7, 120.2, 123.6, 125.3, 127.5, 129.4, 130.7, 131.7, 132.1, 133.5, 135.4, 144.1, 155.2, 158.4, 159.6, 190.3, 202.5, 204.7 ppm. Anal. Calcd. for $C_{34}H_{30}NO_3Cl$: C, 76.18; H, 5.64; N, 2.61. Found: C, 76.05; H, 5.72; N, 2.75.

(3-Nitrophenyl) spiro[acenaphthylene-1,9'-acridine] trione (4j). Orange solid, m. p. > 300 °C. IR (KBr) υ: 3594, 3451, 3324, 2935, 1714, 1604 cm^{-1}; ^{1}H NMR (400 MHz, DMSO-d_6) δ: 7.82 (d, 2H, ArH), 7.55 (d, 3H, ArH), 7.37 (d, 3H, ArH), 7.24 (d, 2H, ArH), 1.85-2.30 (m, 8H, $4CH_2$), 0.96-1.15 (m, 12H, $4CH_3$) ppm; ^{13}C NMR (100 MHz, DMSO-d_6) δ: 28.1, 32.1, 44.7, 45.4, 53.8, 109.9, 112.2, 118.4, 121.2, 123.6, 125.4, 128.1, 128.7, 129.4, 131.4, 132.1, 134.6, 136.7, 143.1, 154.5, 155.4, 159.6, 195.3, 202.5, 205.2 ppm. Anal. Calcd. for $C_{34}H_{30}N_2O_5$: C, 74.71; H, 5.53; N, 5.12. Found: C, 74.59; H, 5.61; N, 4.98.

(2,4-Dimethylphenyl) spiro[acenaphthylene-1,9'-acridine] trione (4k). Orange solid, m. p. > 300 °C. IR (KBr) υ: 3604, 3425, 3328, 2937, 1722, 1608 cm^{-1}; ^{1}H NMR (400 MHz, DMSO-d_6) δ: 6.68-8.29 (m, 9H, ArH), 1.14-2.05 (m, 8H, $4CH_2$), 0.73-1.12 (m, 12H, $4CH_3$) ppm; ^{13}C NMR (100 MHz, DMSO-d_6) δ: 27.2, 33.1, 43.7, 45.4, 54.8, 108.9, 113.2, 119.4, 122.2, 124.6, 126.4, 127.1, 128.7, 129.7, 130.4, 132.1, 133.6, 135.7, 142.1, 153.5, 156.4, 158.6, 196.3, 204.5, 205.7 ppm. Anal. Calcd. for $C_{36}H_{36}NO_3$: C, 81.63; H, 6.66; N, 2.64. Found: C, 81.50; H, 6.51; N, 2.79.

(Benzyl) spiro[acenaphthylene-1,9'-acridine] trione (4l). Orange solid, m. p. > 300 °C. IR (KBr) υ: 3351, 3243, 2840, 1652, 1604 cm^{-1}; ^{1}H NMR (400 MHz, DMSO-d_6) δ: 8.34 (s, 1H, ArH), 8.27 (s, 1H, ArH), 8.07 (1, 1H, ArH), 7.80 (d, *J* = 7.2 Hz, 2H, ArH), 7.33 (d, *J* = 7.8 Hz, 2H, ArH), 7.21 (t, *J* = 7.8 Hz, 3H, ArH), 6.97 (s, 1H, ArH), 2.02-2.36 (m, 8H, $4CH_2$), 1.93 (s, 2H, CH_3), 0.96-1.13 (m, 12H, $4CH_3$) ppm; ^{13}C NMR (100 MHz, DMSO-d_6) δ: 27.6, 33.1, 46.1, 52.4, 55.8, 56.3, 109.7, 114.1, 120.3, 122.8, 123.0,

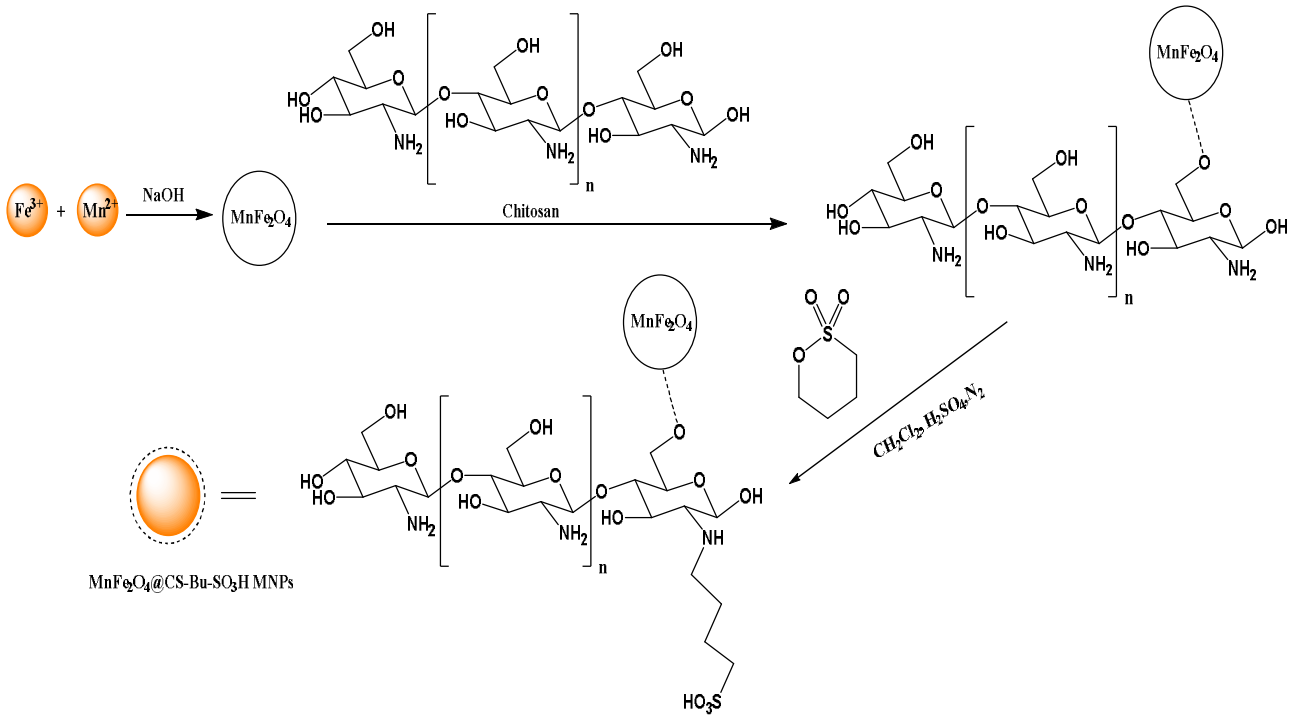

Scheme 1. Preparation steps of $MnFe_2O_4$@CS-Bu-SO_3H MNPs

126.5, 127.9, 129.9, 130.6, 131.1, 132.6, 134.8, 139.7, 142.0, 156.6, 158.1, 167.6, 194.3, 204.5, 206.7 ppm. Anal. Calcd. for $C_{35}H_{33}NO_3$: C, 81.52; H, 6.45; N, 2.72. Found: C, 81.38; H, 6.34; N, 2.61.

RESULTS AND DISCUSSION

Preparation and Characterization of $MnFe_2O_4$@CS-Bu-SO_3H MNPs

The Manganese ferrite nanoparticles were prepared by co-precipitation of Fe(III) and Mn(II) co-precipitation with molar ratio 2:1 then dropped slowly into NaOH solution at temperature of 97 °C. Then, the synthesized magnetic nanoparticles were modified with chitosan as a natural polymer. The modified $MnFe_2O_4$-chitosan nanoparticles, $MnFe_2O_4$ nanoparticles were dispersed in distilled water under ultrasound irradiation, and chitosan in acetic acid solution was slowly added under vigorous stirring for 1 h (Scheme1).

The magnetically heterogeneous organocatalyst, $MnFe_2O_4$@CS-Bu-SO_3H NPs, is characterized by X-ray diffraction (XRD), scanning electron microscopy (SEM), energy-dispersive X-ray spectroscopy (EDX), vibrating sample magnetometer (VSM), thermal gravimetric analysis (TGA), and Fourier transform infrared (FT-IR) spectroscopy.

FT-IR analysis. The FT-IR spectra of (a) chitosan, (b) $MnFe_2O_4$, (c) $MnFe_2O_4$@CS MNPs, and (d) $MnFe_2O_4$@CS-Bu-SO_3H MNPs are instructive (Fig. 1). The O-H stretching vibration at 3428 and 3433 cm^{-1} were detected in peaks of Fig. 1 (a,b,c,d). The FT-IR spectra of chitosan were characterized by the following absorption bands: (NH) of backbone polymer arising at 3435 and 1630 cm^{-1}, (C-O) of primary alcoholic group at 1382 cm^{-1}, and the (C-H) at 2940 cm^{-1} (Fig. 1a). FT-IR spectra of $MnFe_2O_4$ showed characteristic peaks at 3427 cm^{-1} and 1630 cm^{-1} which were assigned to the vibration of hydroxyl groups. In addition, an obvious peak at 584 cm^{-1} was attributed to Fe-O bond vibration (Fig. 1b). Compared to the curve b, in the curve c, the shift of the band, from 584 to 657 cm^{-1}, related to the Fe-O stretching is significant, indicating that iron ions have bound to the NH_2 group of chitosan. Electrostatic interaction between the negatively charged $MnFe_2O_4$ nanoparticles surface and the positively protonated chitosan

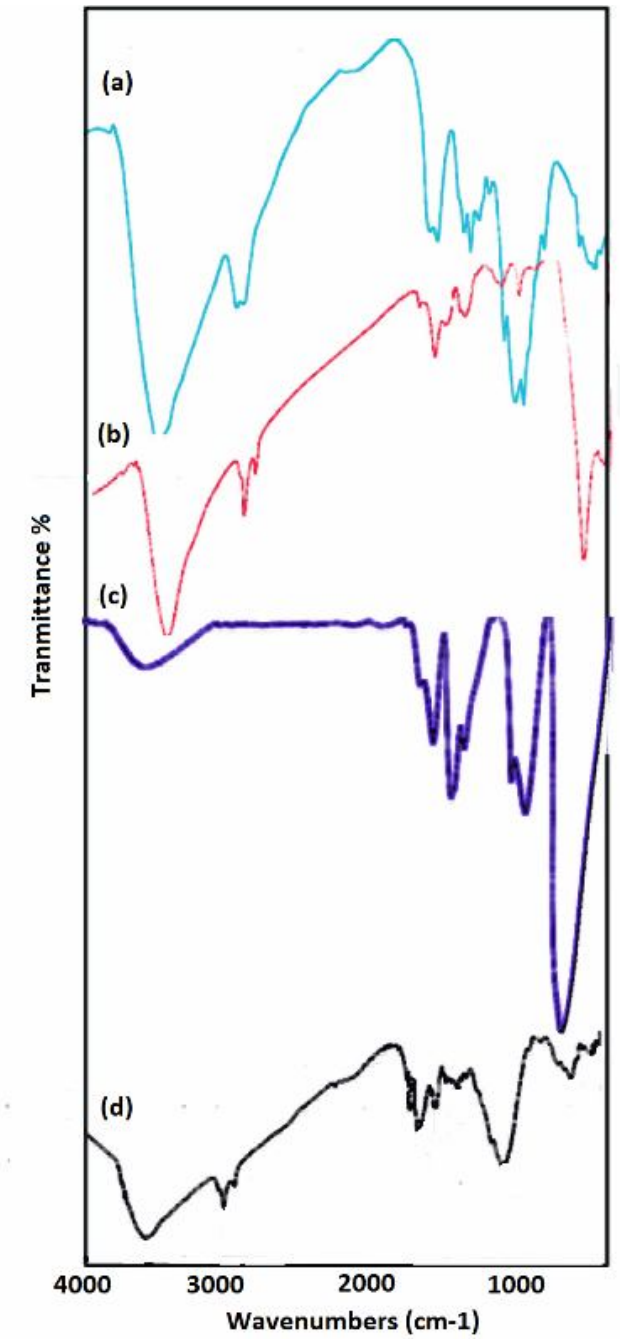

Fig. 1. IR spectra of (a) chitosan (CS), (b) $MnFe_2O_4$, (c) $MnFe_2O_4$@CS MNPs, (d) $MnFe_2O_4$@CS-Bu-SO_3H MNPs.

also donates to the IR change. The peak at 3412 cm^{-1} was probably attributed to the amino group of chitosan, which is overlapped by the O-H stretching vibration of $MnFe_2O_4$ nanoparticles (Fig. 1c). The FT-IR spectrum of $MnFe_2O_4$@CS-Bu-SO_3H MNPs shows the stretching and out-of-plane bending of acidic O-H groups as two broad

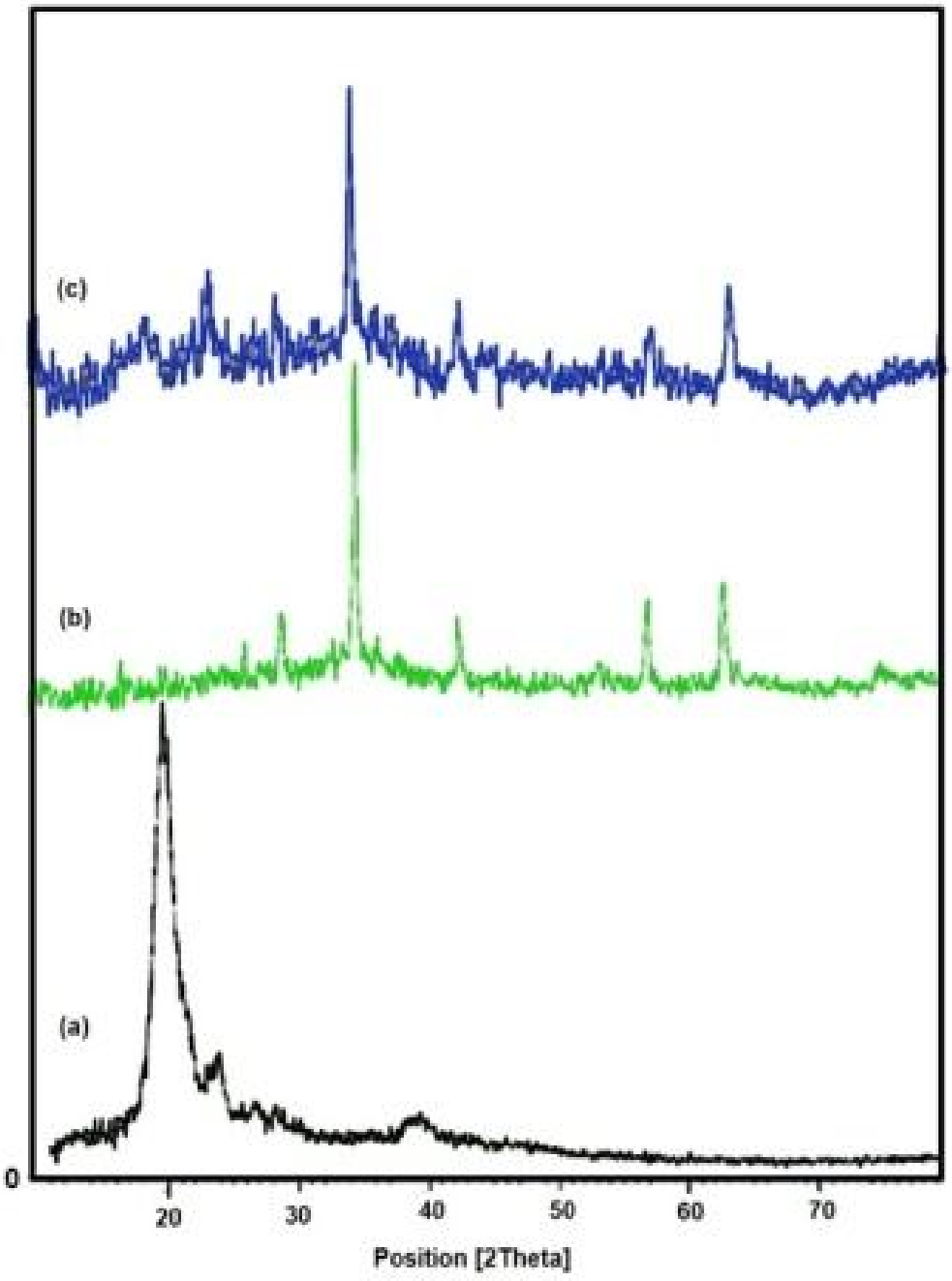

Fig. 2. XRD pattern of (a) chitosan (CS), (b) $MnFe_2O_4$, and (c) $MnFe_2O_4$@CS-Bu-SO_3H MNPs.

bands at 2800-3500 cm^{-1}. Finally, S-O stretching bands of -SO_3H in O-SO_3H and NH-SO_3H groups appeared at 1169 cm^{-1} and 1087 cm^{-1}, respectively (Fig. 1d).

X-ray diffraction (XRD) analysis. The crystal structures of chitosan and $MnFe_2O_4$@CS-Bu-SO_3H MNPs are shown in (Fig. 2). The sharp peaks in the XRD patterns confirm the good crystallinity of the prepared samples. There are six diffraction peaks at 2θ about 29.94°, 35.24°,

42.75°, 52.94°, 56.42° and 61.86 corresponding to (220), (311), (400), (422), (511), and (440) in the $MnFe_2O_4$@CS-Bu-SO_3H MNPs, which is the standard pattern for crystalline magnetite with cubic structure (JCPDS card no. 01-1111). The small and weak broad bands in the range of 12-20° show the existence of amorphous chitosan. The average crystal size of pure $MnFe_2O_4$ and chitosan-coated $MnFe_2O_4$ nanoparticles are 19 and 25, respectively.

Magnetic properties. The magnetization curves for $MnFe_2O_4$ nanoparticles and $MnFe_2O_4$@CS-Bu-SO_3H MNPs nanoparticles are shown in Fig. 3. Room temperature specific magnetization (M) *versus* applied magnetic field (H) curve measurements of the $MnFe_2O_4$@CS-n-Butyle SO_3H NPs nanoparticles indicate a saturation magnetization value (Ms) of 10.27 emu g^{-1}, lower than that of pristine $MnFe_2O_4$ nanoparticles (12.69 emu g^{-1}) due to the coated shell.

Scanning electron microscopy (SEM). Figure 4 exhibits the morphology and particle size of $MnFe_2O_4$@CS-Bu-SO_3H MNPs. It indicates that the chitosan polymeric matrix is uniformly covered on the surface of $MnFe_2O_4$ (Fig. 4). The SEM image shows that the structure of $MnFe_2O_4$@CS-Bu-SO_3H size is bigger. The SEM of $MnFe_2O_4$@CS-Bu-SO_3H MNPs clearly revealed the structure of the CS-coated magnetite nanoparticle.

Energy dispersive X-ray (EDX). The elemental compositions are calculated from the energy dispersive X-ray (EDX). The elemental compositions of $MnFe_2O_4$@CS-Bu-SO_3H MNPs are 3.01%, 11.56%, 6.83%, 29.73%, 30.74% and 18.12% for N, C, S, O, Fe and Mn, respectively. This implied that chitosan polymer was coated on the surface of the $MnFe_2O_4$ NPs (Fig. 5).

Thermal gravimetric analysis (TGA). In order to obtain information on the thermal stability, TGA experiments were carried out by heating $MnFe_2O_4$@CS-Bu-SO_3H MNPs up to 800 °C (Fig. 6). The weight loss of $MnFe_2O_4$@CS-Bu-SO_3H MNPs nanoparticles is about 40% at 250-420 °C, corresponding to the thermal decomposition of chitosan chains over $MnFe_2O_4$ nanoparticles.

Synthesis of Spiroacridines

After the characterization of the catalyst, the reactions of dimedone (2 mmol), aniline (1 mmol), and acenaphthoquinone (1 mmol) were investigated in the presence of $MnFe_2O_4$@CS-Bu-SO_3H MNPs (Scheme 2) in order to optimize the reaction parameters.

The model reaction was examined in the presence of different amounts of $MnFe_2O_4$@CS-n-Butyle SO_3H NPs at various temperatures and also under ultrasonic irradiation in various solvents. The results are shown in Table 1, entry 3. As this table indicates, the best results were obtained when the reaction was performed using 1mg of the catalyst in EtOH/H_2O under ultrasonic irradiation.

Moreover, in order to investigate the effects of ultrasonic irradiation and to evaluate and compare conventional heating or silent with ultrasound assisted method, we continued our efforts under different conditions. The results were listed in Table 1 (entries 3,4). It is notable that the corresponding products were obtained in excellent yields and short reaction times under ultrasonic irradiation. Ultrasound enhances the chemical reactions in a solution through the generation of cavitations micro bubbles. Therefore, the ultrasound can be raised the rate of reaction and so reduce the energy consumption. The chemical and physical effects of ultrasound are primarily originated from sonic cavitation, including formation, growth and collapse of the hole.

We employed various conditions and it was found that the reaction gives satisfying result in the presence of 3 mg of $MnFe_2O_4$@CS-Bu-SO_3H MNPs under ultrasonic irradiation with the power of 35W in aqueous ethanol.

We also applied $MnFe_2O_4$@CS-Bu-SO_3H MNPs in synthesis of spiroacridines from various aromatic amines under similar conditions as represented in Table 3. In general, the reactions are clean and high-yielding. Several groups, such as Cl, Br, NO_2, OCH_3, OH and CH_3, are compatible under the reaction conditions. Interestingly, a variety of aromatic amines, including *ortho*, *meta* and *para*-substituted aryl amines participated well in this reaction and gave the corresponding products in a good to excellent yield (Table 3). The influence of electron-withdrawing and electron-donating substituents on the aromatic ring of amines upon the reaction yields was investigated. These results show that aromatic amines with electron-releasing groups reacted faster than those with electron-withdrawing groups.

The proposed reaction mechanism for the synthesis of spiroacridines catalyzed by $MnFe_2O_4$@CS-Bu-SO_3H MNPs

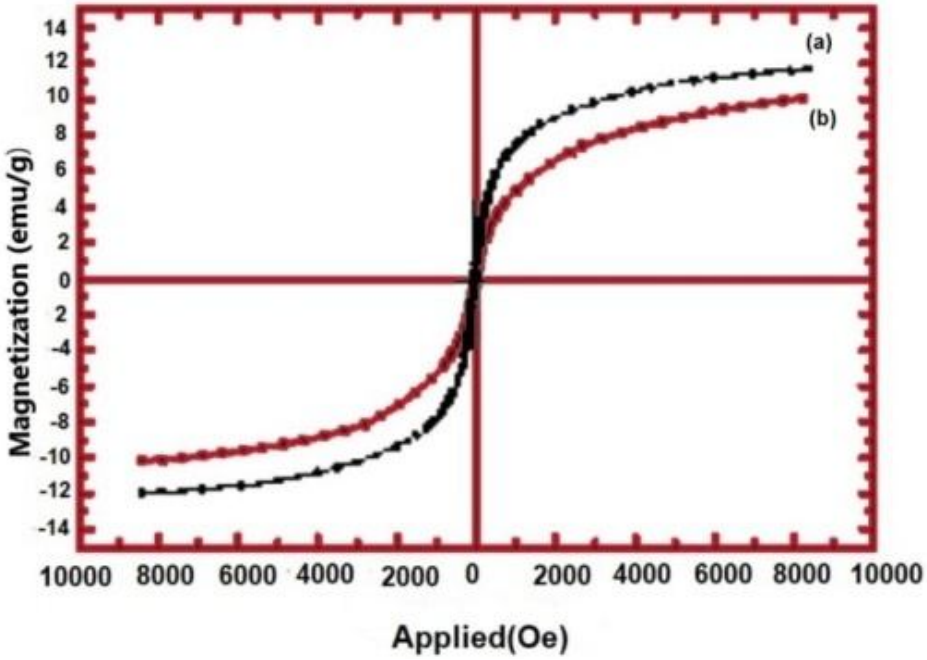

Fig. 3. VSM of (a) $MnFe_2O_4$, and (b) $MnFe_2O_4$@CS-Bu-SO_3H MNPs.

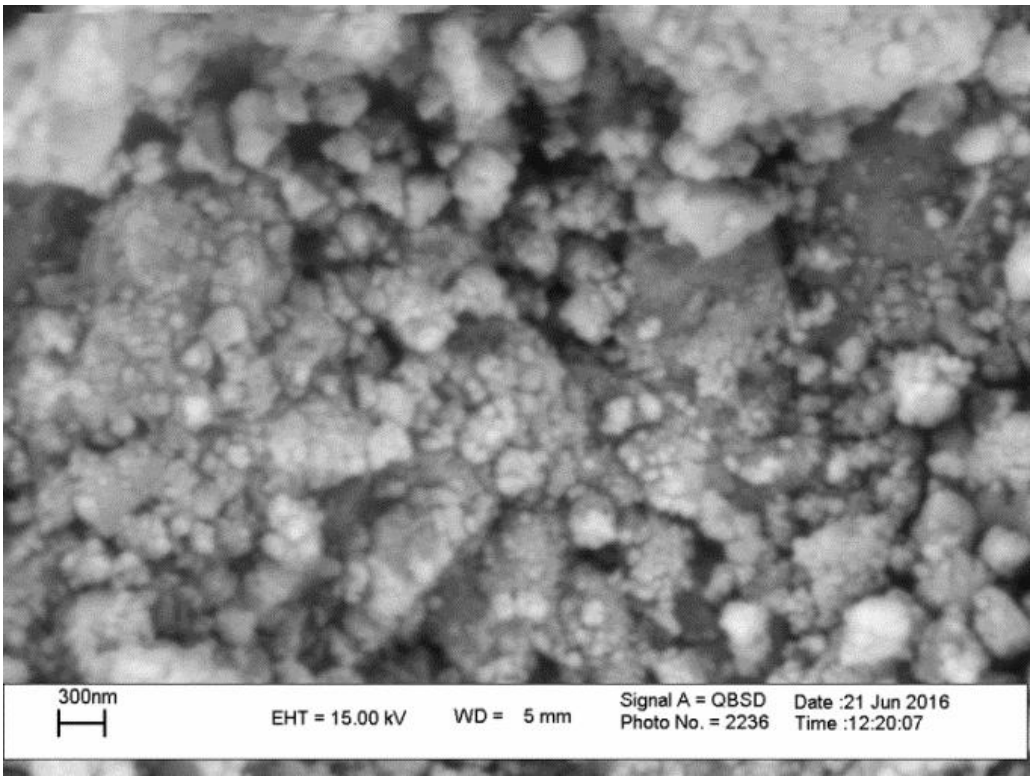

Fig. 4. SEM image of $MnFe_2O_4$@CS-Bu-SO_3H MNPs.

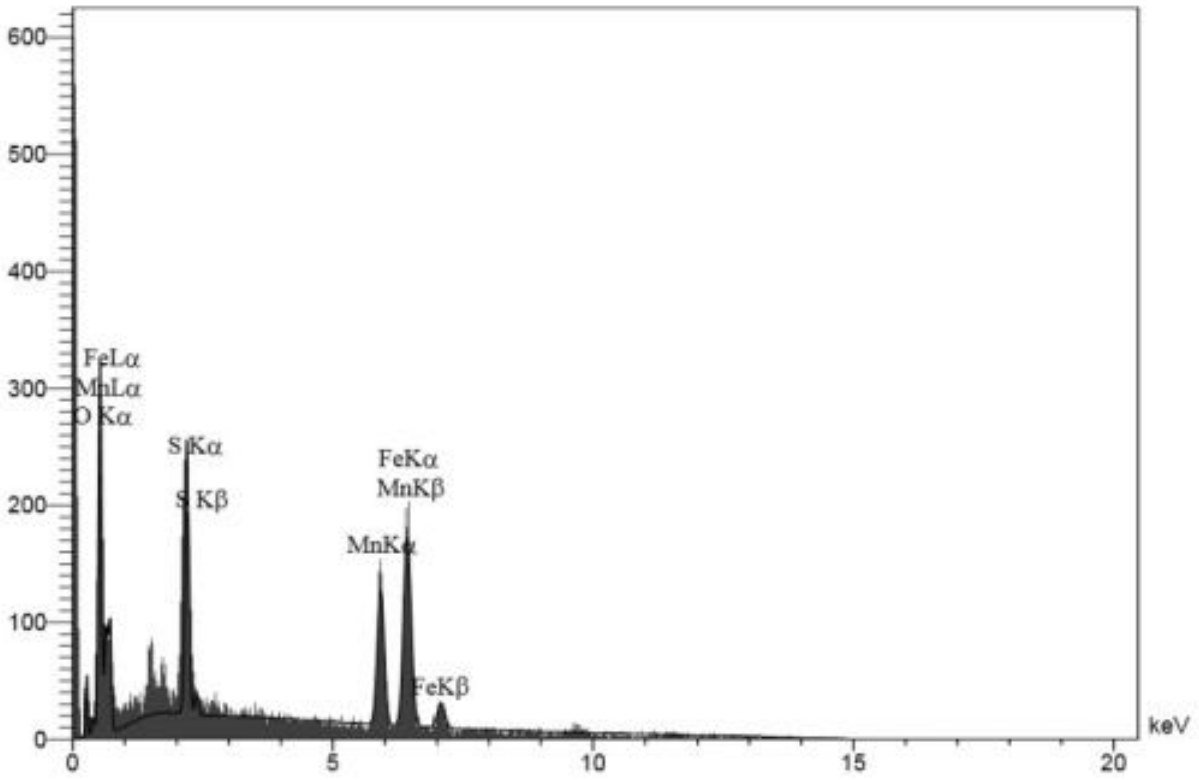

Fig. 5. The EDX of $MnFe_2O_4$@CS-Bu-SO_3H MNPs.

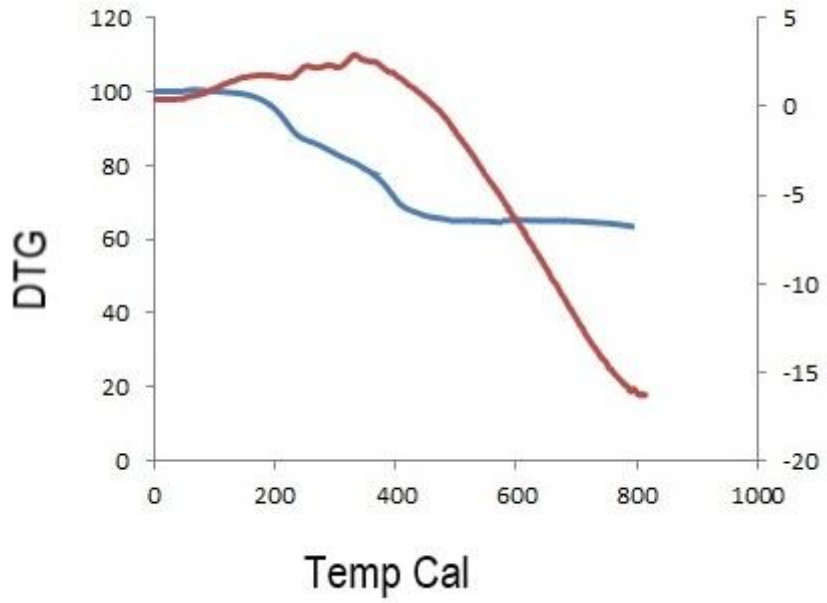

Fig. 6. The thermal gravimetric analysis (TGA) of $MnFe_2O_4$@CS-Bu-SO_3H MNPs.

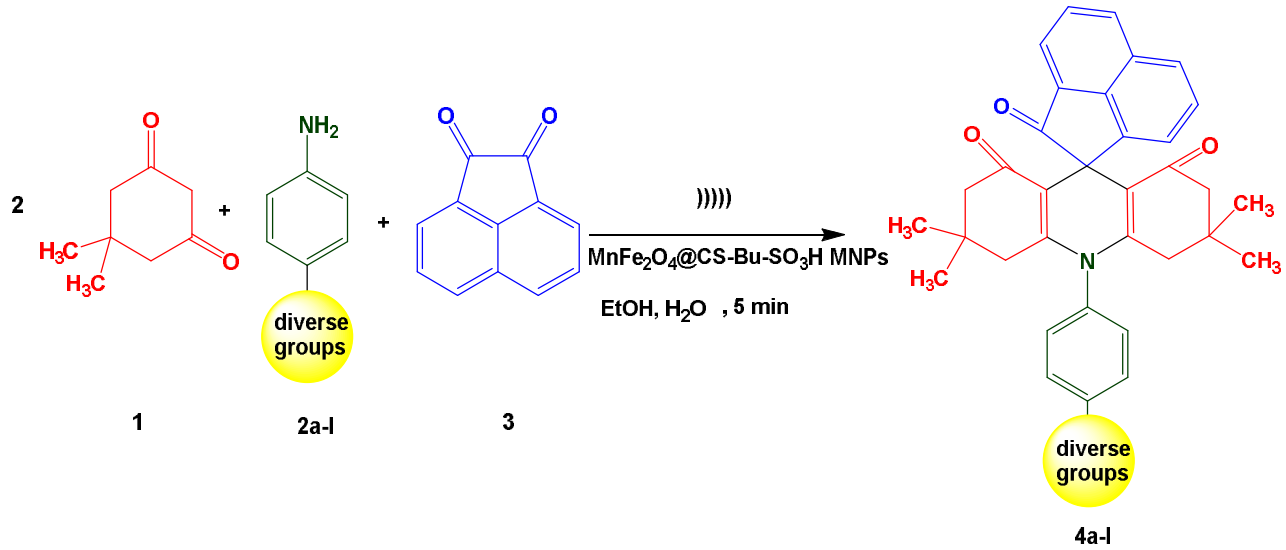

Scheme 2. Synthesis of spiro[acenaphthylene-1,9'-acridine] trione catalyzed by $MnFe_2O_4$@CS-Bu-SO_3H MNPs

Table 1. Optimizing the Synthesized Spiroacridines in the Presence of Different Conditions

Entry	$MnFe_2O_4$@CS-n-Bu-SO_3H NPs (mg)	Solvent	Heating condition	Ultrasonic irradiation
			Time (h)/Yield (%)[a]	Time (min)/Yield (%)[a]
1	0.3	EtOH/H_2O	2/54	15/75
2	0.5	EtOH/H_2O	2/59	15/75
3	2	EtOH/H_2O	1/63	4/94
4	3	EtOH/H_2O	1/63	4/94
5	2	CH_3CN	2/42	25/52
6	2	H_2O	2/-	25/-
7	-	EtOH/H_2O	4/Trace	40/40

[a]Isolated yields.

is depicted in Scheme 3. Initially, the $MnFe_2O_4$@CS-Bu-SO_3H MNPs catalyst protonates the carbonyl group of acenaphthoquinone (1), which then is condensed with CH acidic group of dimedone (2) through a fast Knoevenagel condensation to afford A derivative. Then, dimedone (2) participates in a Michael addition with compound A to form intermediate B. The -NH group of amine then undergoes an intramolecular attack of the carbonyl group resulting in a cyclization reaction that affords C. Finally, intermediate C loses a molecule of H_2O to lead to the formation of acridine D.

The reusability of the catalyst is an important benefit for

Table 2. The Effect of Ultrasonic Irradiation on the Formation of Spiroacridines[a]

Entry	Power (w)	Time (min)	Yield (%)[b]
1	15	30	54
2	20	20	71
3	30	15	80
4	35	4	94
5	40	4	94

[a]Dimedone (2 mmol), aniline (1 mmol), acenaphthoquinone (1 mmol) and $MnFe_2O_4$@CS-Bu-SO_3H MNPs (3 mg). [b]Isolated yields.

Table 3. Synthesis of Various Spiroacridines Using $MnFe_2O_4$@CS-Bu-SO_3H MNPs under Ultrasonic Irradiation (35W)

Entry	Product	Amine (X)	Time (min)	Yield (%)[a]
1	4a	4-NO_2	8	85
2	4b	4-OH	5	93
3	4c	4-Cl	6	87
4	4d	4-Br	6	89
5	4e	4-Me	5	91
6	4f	4-OMe	5	93
7	4g	2-OH	5	90
8	4h	2-NO_2	8	83
9	4i	2-Cl	6	80
10	4j	3-NO_2	9	76
11	4k	2,4-Me_2	5	92
12	4l	Benzyl	7	88

[a]Isolated yield.

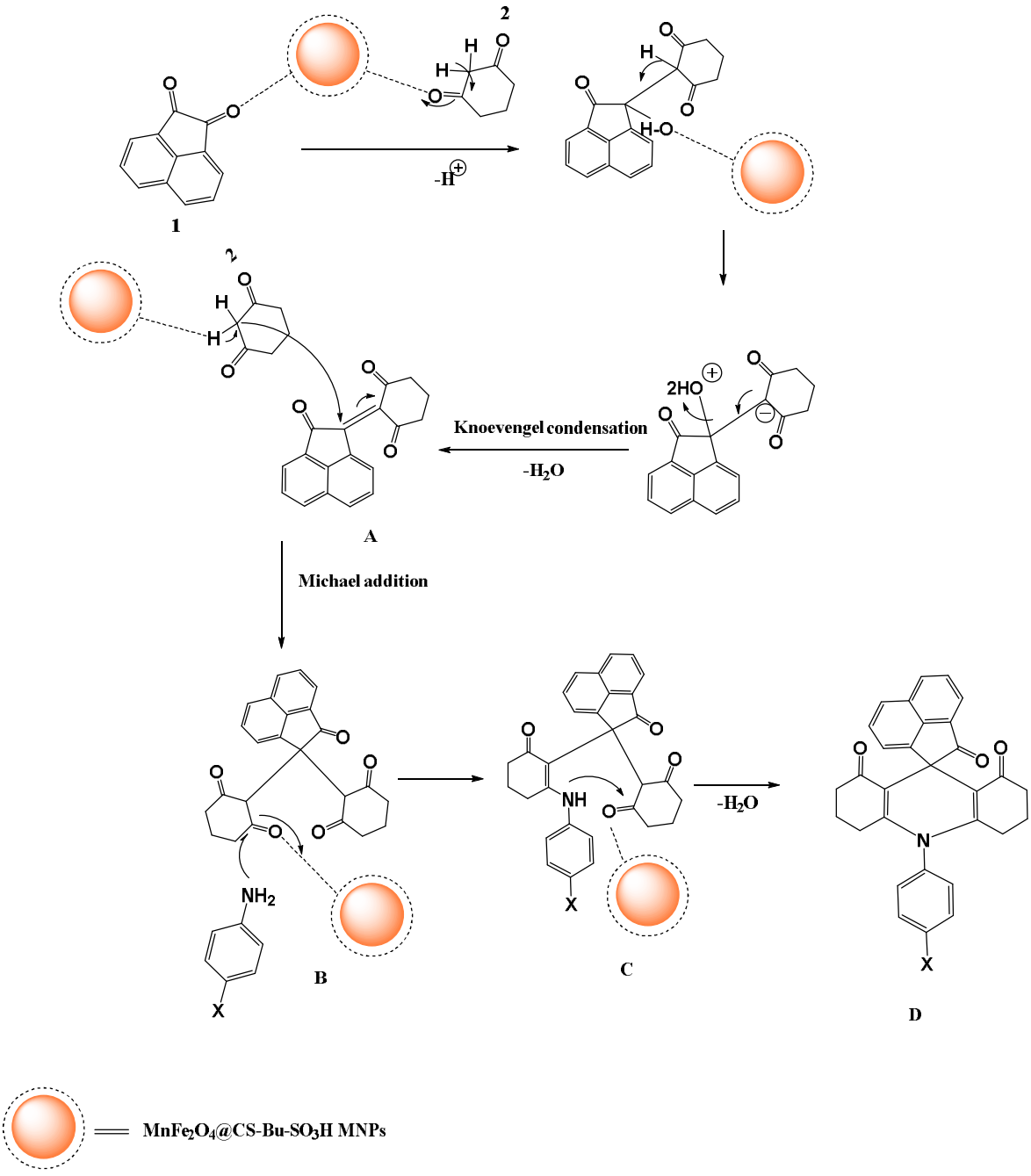

Scheme 3. Plausible mechanism for the synthesis of spiroacridine

catalytic reactions. The reusability was investigated using the reaction of dimedone, aniline and acenaphthoquinone in the presence of $MnFe_2O_4$@CS-Bu-SO_3H MNPs under optimized conditions (Fig. 7). The catalyst was recovered by an external magnet and washed three times with water-acetone, dried and then reused for subsequent reactions for at least 5 times with less reduction in its catalytic activity.

For the characterization of $MnFe_2O_4$@CS-Bu-SO_3H MNPs, the SEM image of catalyst after five times of reuse was shown the same particle size (Fig. 8). Interestingly, the

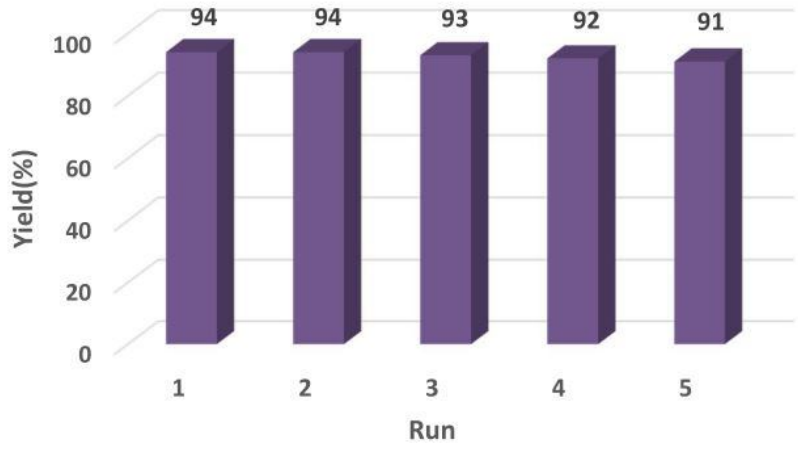

Fig. 7. Reusability of catalyst for the synthesis of spiroacridine.

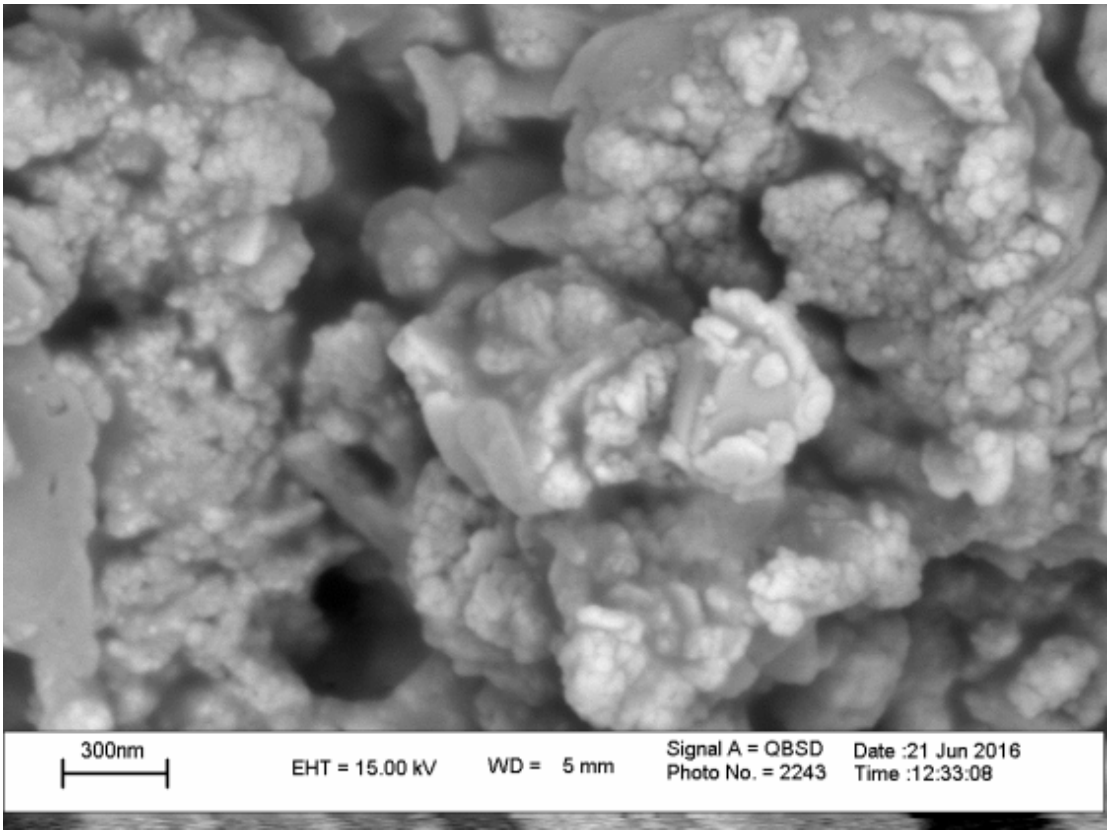

Fig. 8. The SEM Image of $MnFe_2O_4$@CS-Bu-SO_3H MNPs after five times reuse.

shape and size of the nanoparticles remained unchanged after reaction. We believe that this is also the possible reason for the extreme stability of the $MnFe_2O_4$@CS-Bu-SO_3H MNPs Presented herein.

CONCLUSIONS

In this research, we have described the synthesis of spiroacridine derivatives using 3 mg $MnFe_2O_4$@CS-Bu-SO_3H MNPs catalyst under ultrasonic irradiation. The catalyst is recyclable and provides excellent yields of spiroacridines. The remarkable advantages of this methodology are easy work-up, short reaction times, recycling of the catalyst, little catalyst loading and use of ultrasonic irradiation as a valuable and powerful technology.

ACKNOWLEDGEMENTS

The authors are grateful to the University of Kashan for supporting this work by Grant no. 159148/88.

REFERENCES

[1] S.J. Tabatabaei Rezaei, M.R. Nabid, A. Yari, S. Weng Ng, Ultrason. Sonochem. 18 (2011) 49.

[2] Gh. Zbancioc, O. Florea, P.G. Jones, I.I. Mangalagiu, Ultrason. Sonochem. 19 (2012) 399.

[3] J.-T. Li, X.-L. Zhai, G.-F. Chen, Ultrason. Sonochem. 17 (2010) 356.

[4] A.R. Suresh Babu, R. Raghunathan, Tetrahedron Lett. 49 (2008) 4618.

[5] P. Shanmugam, B. Viswambharan, K. Selvakumar, S. Madhavan, Tetrahedron Lett. 49 (2008) 2611.

[6] P. Shanmugam, B. Viswambharan, S. Madhavan, Org. Lett. 9 (2007) 4095.

[7] C. Mustazza, A. Borioni, I. Sestili, M. Sbraccia, A. Rodomonte, R. Ferretti, M.R. Del Giudice, Chem. Pharm. Bull. 54 (2006) 611.

[8] D. Rambabu, S. Kiran Kumar, B.Y. Sreenivas, S. Sandra, A. Kandale, P. Misra, M.V. BasaveswaraRao, M. Pal, Tetrahedron Lett. 54 (2013) 495.

[9] A. Maleki, M. Kamalzare, M. Aghaei, J. Nanostruct. Chem. 59 (2015) 5.

[10] M.B. Gawande, A.K. Rathi, I.D. Nogueira, R.S. Varma, Paula S. Branco, Green Chem. 7 (2013).

[11] D. Wang, D. Astruc, Chem. Rev. 114 (2014) 6949.

[12] F. Shirini, M. Abedini, J. Nanosci. Nanotechnol. 13 (2013) 4838.

[13] H. Montazeri1, A. Amani, H.R. Shahverdi, E. al din Haratifa, A.R. Shahverdi, J. Nanostruct. Chem. 3 (2013) 1.

[14] R.M Wang, N.-P He, P.-F. Song, Y.-F. He, L. Ding, Z. Q. Lei, Polym. Adv. Technol. 20 (2009) 959.

[15] M. Adlim, M.A. Bakar, K. Yong Liew, J. Ismail, J. Mol. Catal., A: Chem. 212 (2004) 141.

[16] A. Maleki, M. Aghaei, N. Ghamari, Chem. Lett. 44 (2015) 259.

[17] Y. Shi, Jimin Du, L. Zhou, X. Li, Y. Zhou, L. Li, X. Zang, X. Zhang, F. Pan, H. Zhang, Z. Wang, X, Zhu, J. Mater. Chem. 22(2012) 355.

[18] H. Naeimi, Kh. Rabiei, Ultrason. Sonochem. 19 (2012) 130.

[19] R. Ghahremanzadeh, Z. Rashid, A.H. Zarnani, H. Naeimi, Ultrason. Sonochem. 21 (2014) 1451.

[20] Kh. Rabiei, H. Naeimi, Ultrason. Sonochem. 24 (2015) 150.

[21] H. Naeimi, A. Didar, Ultrason. Sonochem. 34 (2017) 889.

[22] H. Naeimi, R. Shaabani, Ultrason. Sonochem. 34 (2017) 246.

[23] H. Naeimi, S. Rahmatinejad, Z.S. Nazifi, J. Taiwan Inst. Chem. Engin. 58 (2016) 1.

[24] R. Ghahremanzadeh, Z. Rashid, A.H. Zarnani, H. Naeimi, Appl. Catal. A: Gen. 467 (2013) 1.

[25] J. Safari, L. Javadian, Ultrason. Sonochem. 22 (2015) 1.